Cement & Concrete Composites 31 (2009) 221–231

Contents lists available at ScienceDirect

Cement & Concrete Composites

journal homepage: www.elsevier.com/locate/cemconcomp

Experimental investigations on the durability of fibre–matrix interfaces in textile-reinforced concrete

Marko Butler, Viktor Mechtcherine *, Simone Hempel

Institute of Construction Materials, TU Dresden, 01062 Dresden, Germany

ARTICLE INFO

Article history:
Received 28 November 2008
Received in revised form 2 February 2009
Accepted 3 February 2009
Available online 12 February 2009

Keywords:
Textile-reinforced concrete
Fibre–matrix interface
Durability
AR-glass

ABSTRACT

Changes in the strength and toughness of textile-reinforced concrete with increasing age are determined essentially by the durability of the armouring fibres, the matrix itself, and the bond between the matrix and the fibres. Based on new experimental results, important mechanisms influencing the durability of the fibre–matrix bond are treated in this article and discussed as to their significance. The investigations were conducted on multi-filament yarns of AR-glass which were imbedded in matrices of varying alkalinity and hydration kinetics. The loading capacity of the fibre–matrix bonds was determined in direct tension tests on under-reinforced specimens after they had undergone accelerated aging. Further, the condition of the microstructure between fibre and matrix was ascertained with both image analysis and analytical procedures. It was concluded that measured reductions in the toughness of the composite material could be attributed to the diminishing protective effect of organic polymer sizing on the surface of the filaments as well as to the disadvantageous new formation of solid hydration phases (mainly Portlandite) in the fibre–matrix interface.

1. Introduction

Textile-reinforced concrete (TRC) is a composite construction material consisting of high performance filament yarns of glass, polymeric, or carbon fibre and a matrix of fine-grained concrete. In the majority of the existing and prospective applications of TRC, fabrics made of glass fibre with a high resistance to alkalis (so-called AR-glass) are used. The main features of TRC are its high tensile strength and its pronounced pseudo-ductile behaviour, i.e., the tolerance of this new material to large deformations. TRC, with its excellent mechanical properties, has many possible applications both in new and old structures as well as in the strengthening and repair of structural elements made of reinforced concrete or other traditional materials [1].

Most of these applications require that the high tensile strength and toughness of TRC do not degrade significantly with increasing age. Possible negative alterations must be known in order to be considered in the design of structural members made of or strengthened with TRC. Changes in the mechanical performance of the composite can result from deterioration of the armouring fibres, alterations in the matrix itself, and changes in the bond between matrix and fibres. This investigation mainly evaluates the mechanisms influencing the performance of the bond and also addresses the influences of organic polymer sizing on the resistance of AR-glass fibre to corrosion. To accomplish this pullout tests on two types of multi-filament yarns embedded in four different matrices were performed. Before testing the specimens were subjected to accelerated aging.

2. Aging of TRC: overview of damage mechanisms

The durability of TRC reinforced with AR-glass fibre multi-filament yarn is governed mainly by the same damage mechanisms as glass-fibre-reinforced concrete (GRC). The following degradation processes are generally reported in the literature:

- Corrosion of the fibre material itself due to attack of OH^- ions in the pore solution [8–12].
- Static fatigue (delayed failure) of the glass fibre under sustained load in the highly alkaline environment [13–16,29–33].
- Densification of the matrix adjacent to the filaments and enhancement of the fibre–matrix bond with continued hydration and precipitation of hydration products in the interface between filaments and matrix as well as in empty spaces between the filaments of multi-filament yarn (bundle filling) [4,17–23,36].

The resistance of the fine-grained concrete matrix itself to environmental influences such as chemical attack or frost certainly also may affect the durability of the composite. However, these kinds of exposure are not covered in this paper.

* Corresponding author. Tel.: +49 351 4636311; fax: +49 351 4637268.
E-mail address: mechtcherine@tu-dresden.de (V. Mechtcherine).

0958-9465/$ - see front matter © 2009 Elsevier Ltd. All rights reserved.
doi:10.1016/j.cemconcomp.2009.02.005

Standard AR-glass contains 16–20% by mass zirconium dioxide and provides therefore a significantly enhanced resistance in highly alkaline environments as compared to conventional glasses [8,9]. The reason for the enhanced alkaline resistance is the formation of a thin hydrated, zirconium-rich layer on the filaments' surfaces as reported by Larner et al. [10] and Yilmaz and Glasser [11]. The layer forms after the beginning of an alkaline attack on the glass network and slows down the diffusion of OH^- ions into the bulk glass. Thus, further network breakdown can be reduced significantly but not completely precluded in high alkaline pore solutions, as shown in [9–12]. The corrosive damage occurs non-uniformly due to different element concentration near the filament surface both in the axial and longitudinal directions. This deterioration increases with increasing pH value of the pore solution and with temperature [11,12]. Organic polymer sizes applied to filament surfaces during the production of glass yarns can significantly delay such corrosion [5,25]. At the outset the thickness (nano-scale) reduces rapidly when in contact with pore solution. This process nearly stops after some time, while approximately 30% of the initial thickness of the size remains at the filament surfaces, offering additional protection to the glass [25].

The strength of glass fibres is significantly reduced by tiny surface defects caused by the fibre spinning process [13] or by chemical attack [14,15]. Stress concentrations arise at the tips of these defects when the filament is strained, e.g., due to the external loading of TRC. The growth of such defects is fostered especially in the case of high constant stresses at the tip and presence of water [14,16], which subsequently lead to a delayed failure of filament, although at the beginning the filament stress was definitely less than critical. An alkaline environment and higher temperatures support the defect growth. According to [26,27], polymer size at the filament surface can reduce stress concentrations at existing defect tips depending on polymer characteristics and defect size. Furthermore, the diffusion of water and OH^- ions to the tip can be delayed due to the defects' being at least partly filled with polymer [26]. Thus, polymer size can enhance the resistance of glass fibre to failure in general and to delayed failure in particular.

An increase in contact area between filaments and matrix in conjunction with increasing bond strength has been reported in many publications and relates not only to glass fibre; see [4,17–23,36]. The interface zone adjacent to the filament is initially porous and becomes denser in the process of cement hydration [19]. Consequences of this densification are increases in shear stress as well as in local bending of filaments which cross matrix cracks non-orthogonally [17,20,21]. This results in the failure of such filaments even at low external loads if brittle fibre materials like glass are used. Furthermore, the growth of brittle shells of hydration products wrapping the filaments is reported in [22]. Under mechanical loading the shells tend to spalling, producing distinct discontinuities in filament-shell cross-section and stiffness. Hence, pronounced stress concentrations occur in the fibre at these locations. Additionally, the precipitation of hydration products within the yarn reduces its flexibility and strengthens the bond to the inner filaments, as shown by Bartos and Zhu [4,23]. In this way sliding of inner filaments relative to outer filaments in multi-filament yarn is strongly reduced or even completely obviated [2,36]. The composition of the precipitated hydration phases is predominantly crystalline $Ca(OH)_2$; see [11,20]. Crystal growth of $Ca(OH)_2$ can cause fibre notching by chemo-mechanical interaction at the fibre surface [11]. Conditions necessary for such damaging epitaxy are enumerated in [24]. The phase changes at the fibre–matrix interface can change the behaviour of the composite from ductile to brittle and can also influence the strength of composite material itself. It should be also noted that the formation of hydration products at the interface is governed by the size applied to filament surfaces or additional polymer coating of multi-filament yarns [5–7,19].

In aging TRC the degradation mechanisms described always occur not in isolation but are contiguous. However, expert opinions on the relative importance of the individual phenomena or processes differ widely.

The delayed failure of glass fibres is supposed to dominate the other mechanisms according to [29–33]. Purnell [29,30] proposed a static fatigue model to explain the losses in strength of artificially aged GRC, which had been described empirically by Litherland's model [28] before. The Purnell model is based on the calculation of the filament strength, as influenced exclusively by defect growth in dependence on the temperature, the OH^- concentration, and the stress level at the defect tip. Purnell assumes that in mechanically unloaded composite stresses can arise, for example, from the different thermal expansion behaviours of matrix and glass or from the nucleation and epitaxy of $Ca(OH)_2$ in the defects' confined spaces. At least the second assumption seems to be improbable, since the contact angles between substrate and crystal are unfavourable within these defects; see [24]. For Portland cement matrices an additional chemical reaction between $Ca(OH)_2$ and filaments is stated, while in matrices with modified composition (addition of pozzolan, etc.) only static fatigue of the glass seems to be responsible for strength losses of composite [30].

Orlowsky et al. [31–33] enhanced the static fatigue model by introducing two reaction rate coefficients. These coefficients describe on the one hand the kinetic part of the defect growth (which is due to reactions between stressed glass and water or OH^-) and on the other hand the diffusion-controlled part of damaging process (transport of water or OH^- to the defect tip, increasingly hindered by the deposit of recondensed silanol groups) [31]. The model parameters were ascertained by fitting to test results obtained for filaments, yarns as well as composite materials subjected to different aging regimes. Modifications to the fibre–matrix interface were not taken into account by this model. This was justified by results obtained from thin-section petrography [34] and crack distance measurements during tensile tests [30] on composites, at which no influence of interface modifications during aging could be ascertained.

However, investigations performed at the Institute of Construction Materials at the TU Dresden indicate that the role of the phase changes in the fibre–matrix interface is much more significant with regard to the changes in mechanical properties of the composite over time, and therefore in respect of TRC durability [12,22]. This paper presents new experimental results which substantiate the importance of considering the interface as one of the major factors influencing long-term mechanical performance. These results were obtained in a project carried out under the aegis of the Collaborative Research Centre SFB 528 "Textile Reinforcement for Structural Strengthening and Retrofitting" financed by the German Research Foundation. A more extended and detailed presentation of the research work can be found in [35].

3. Materials and test methods

3.1. Glass fibre

As the reinforcing material used in the investigations, two multi-filament yarns of AR-glass (type CEMFIL, manufacturer Saint Gobain Vetrotex), denoted as VET-02 and VET 03, respectively, were selected from directly adjacent production runs. The multi-filament yarns consisted of 1600 individual filaments with a diameter of approximately 14 μm, produced in a spinning process out of one glass melt. Immediately after withdrawal from the extrusion jets, the filaments were coated with a thin polymer size.

The size is applied mainly for technological reasons in order to optimise the processing of the filaments to yarns. However, as

mentioned before, the size covers defects (nanoscopic flaws) arising from the manufacturing process in the glass [13], thereby reducing the tendency of the filaments to break [7,26,27]. Beyond that, it acts as a protective layer over the glass and so improves its resistance to aggressive chemical agents and defines the surface reaction (hydrophilic, hydrophobic, etc.) of the filaments [5,7,25].

Following the application of the size the filaments were spun into 'strands' and subsequently into multi-filament yarns and then spooled. The only partly dried size was cured after spooling by a thermal treatment. The manufacturer provided no information with regard to the composition and properties of the size. Table 1 gives the characteristic properties of the filaments and of the multi-filament yarns.

3.2. Matrix material – fine-grained concrete

Four concrete compositions, designated M1, M3, M7 and M45, were used in this investigation as matrix material. All four concretes had a maximum particle size of 1 mm and high binder content. Each differentiated itself from the others with respect to alkalinity, hydration kinetics, and granulometry of the binder. Table 2 gives the compositions of the matrices.

Matrix M7 represents with respect to its high alkalinity an extreme case in assessing the durability of composite material. The binder consists entirely of Portland cement, and there is no buffering of the alkalinity by pozzolanic additives. In contrast, the binder of Matrices M1 and M45 consists of a blast furnace cement rich in ground granulated blast furnace slag with a strong buffering of the alkalinity through the addition of fly ash and microsilica (composition M1) or metakaolin (composition M45). The only difference between the compositions M1 and M45 is that for M45 microsilica suspension was replaced by metakaolin powder, while the amount of the mixing water was increased in order to "replace" the water contained in the microsilica suspension (composition M1). Matrix M3 should be seen in respect of both its alkalinity and hydration kinetics to be between Matrices M7 and M1 (or M45).

Fig. 1 shows the development of pH values of these matrices over time. The specimens, concrete prisms produced for this purpose, were subjected to accelerate aging in a fog-room (40 °C, 99% RH). One year of aging is estimated to simulate correctly the changes in a matrix as in approximately 50 years of storing in ordinary middle-European climates. The measurements of pH were performed for all four compositions on filtered slurry of dry ground matrix material, which was taken from inner parts of the concrete prisms. To produce the slurry, 10 g matrix powder were mixed with 50 ml distilled water. Additionally, the pH values of pore solution of Matrices M1 and M7 were measured for the sake of comparison and as a more direct indicator. For this purpose some drops of pore solution were pressed out of the fine crushed matrix material filled in a special steel cylinder.

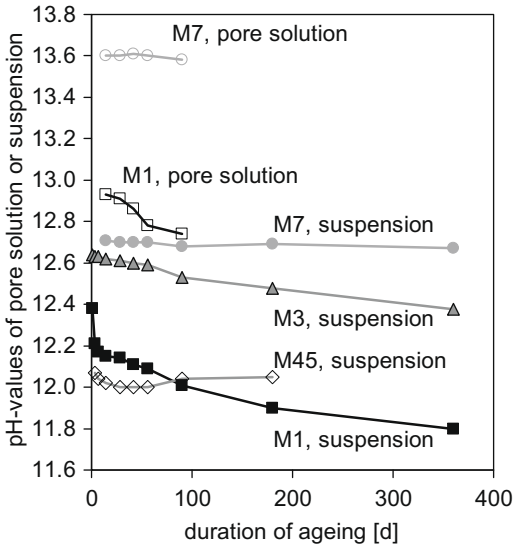

Fig. 1. Development of pH values over time for the matrices investigated.

The results obtained from the measurements show a pronounced reduction in the pH level with increasing matrix age for the matrices containing pozzolanic components. The decrease in the pH value of Matrix M45 is very prominent during the initial days of accelerated aging. The pH level, however, stabilizes after approximately one month of storing the fog chamber. Matrix M1 provides a more continuous consumption of alkalines, which leads to pH values of approximately 11.8 after 360 days of aging. In contrast, Matrix M7, which contains no pozzolans, exhibits a nearly constant pH level during the entire time span of the investigation. The development of pH values in Matrix M3 is, as could be expected on the basis of its composition, somewhere between the trends observed for Matrices M1 and M7.

3.3. Test sample geometry and fabrication

To investigate the mechanisms which lead to an alternation of the mechanical performance of textile-reinforced concrete, a test setup is needed which excludes various artefacts resulting from a complex geometry of the technical textiles, thus allowing possibly a straightforward interpretation of the results obtained. Since the bond and pullout behaviour of multi-filament yarn embedded in fine-grained concrete appears to be definitive of the strength and deformation properties of TRC, double-sided pullout tests as described below were developed and applied in this study.

Doubly symmetrical, narrowed prisms scored with a defined break cross-section (notch of depth 1 mm, Fig. 2) were used as specimens. In the vicinity of the notch each specimen was 5 mm thick, and at the ends the thickness increased to 10 mm. The width of the samples was 50 mm. Each specimen was reinforced with three multi-filament yarns, which were extended over the entire

Table 1
Properties of filaments and multi-filament yarns.

Description	Filament		Multi-filament yarn	
	VET-02	VET-03	VET-02[a]	VET-03[b]
Number of filaments	1	1	1600	1600
Fineness (tex)[c]	0.391	0.399	640	665
Diameter (μm)	13.43	13.59	–	–
Tensile strength (MPa)	1721	1917	1195	1445
Strain-capacity (%)	2.36	2.58	2.09	2.18

[a] Yarn ARG-VET640-02 (nomenclature SFB 528).
[b] Yarn ARG-VET640-03 (nomenclature SFB 528).
[c] Mass in g of 1 km yarn or filament, respectively; (tex = g/km).

Table 2
Compositions of the fine-grained concretes, masses in kg per m^3 of concrete.

Matrix composition	M1 (kg/m^3)	M3 (kg/m^3)	M7 (kg/m^3)	M45 (kg/m^3)
CEM I 32.5 R	–	557	861	
CEM III/B 32.5 NW-HS-NA	550	–	–	551
Fly ash	248	251	–	248
Microsilica suspension (50 mass% powder, 50 mass% water)	55	56	–	–
Metakaoline				28
Sand 0–1 mm	1101	1114	1148	1101
Water	248	251	287	275

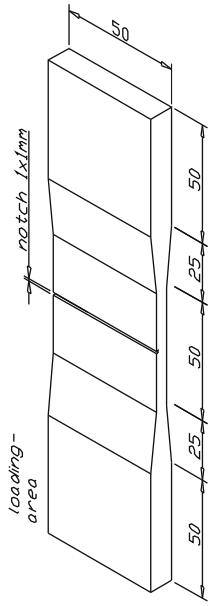

Fig. 2. Dimensions of the specimen for double-sided pullout test.

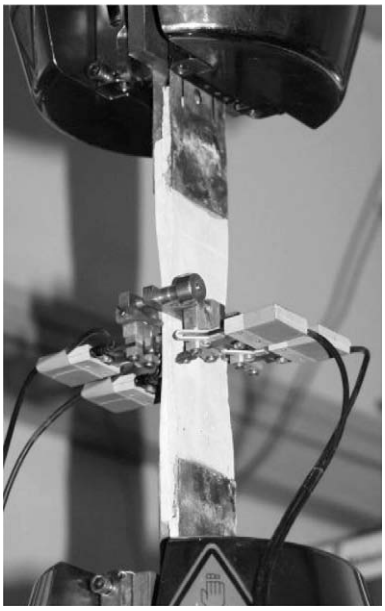

Fig. 3. Mounted specimen with load application grips and crack width sensors.

length of the sample parallel to each other at a distance of 10 mm. Prior to concreting, the reinforcing yarns were fixed on a stretching frame in order to imbed them tautly into the fine-grained concrete. The degree of reinforcement was selected in such a manner as to allow only simple crack formation at the weakest cross-section, thus as a rule avoiding multiple cracking. The fibre volume content in the notch cross-section was 0.105%.

Keeping the defined conditions during the entire fabrication, storage and testing were absolute prerequisites for achieving reproducible results. The specimens were formed in completely enclosed moulds so that uniform conditions in fabrication and at the same time an identical geometry of the samples were assured. The specimens were removed from their moulds one day after fabrication and with that the imbedded reinforcing yarns were detached from the mounting frame. Subsequently the specimens were stored until an age of 7 days in water at 20 °C. After that a portion of the samples were subjected to accelerated aging in a fog chamber at a temperature of 40 °C and 99% relative humidity. Some reference specimens were stored in the standard laboratory atmosphere at 20 °C and 65% relative humidity. The accelerated aged samples were removed from the fog chamber 3 days prior to testing and conditioned at 20 °C and 65% relative humidity until testing.

3.4. Test procedure

For the double-sided pullout tests, slit steel plates were glued to the loading areas of the specimens and then fixed between the clamping jaws of the testing machine. In this way a nearly unconstrained mounting of the specimens was possible. Fig. 3 illustrates the test arrangement.

The mechanical testing was conducted under a deformation control regime in a servo-hydraulic universal machine. As long as the fine-grained concrete was not yet cracked (Zone I in Fig. 4), the deformation rate was kept 0.05 mm/min. The test rate was increased to 1 mm/min after cracking at the notch cross-section had occurred (cf. Zone II and Zone III in Fig. 4). The test was stopped when a crack-opening of 2.5 mm had been reached. Values of test force, crack width, and displacement of the crosshead of the testing machine were measured and recorded. The measurement of crack width was accomplished by means of precision gauges fixed in the vicinity of the crack (cf. Fig. 3). For each combination of matrix and yarn 10 specimens were tested, except for Matrix M3 and Yarn VET-02, for which only six samples were investigated.

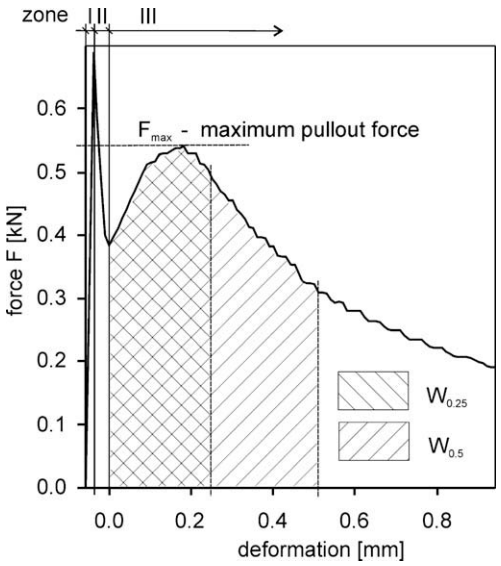

Fig. 4. Schematic representation of complete load–deformation curve with indication of characteristic values F_{max}, $W_{0.25}$, and $W_{0.5}$.

After testing the fibre–matrix interface was investigated under an electron-microscope (ESEM) using micrographs as well as qualitative and quantitative EDX analysis. For this purpose sections of 10 mm length separated from the specimen were laid open along the line of the multi-filament yarn.

4. Results

4.1. Presentation of results

Fig. 4 is the schematic representation of a complete load–deformation curve as measured in the double-sided pullout test. Three zones of the graph can be distinguished depending on the degree

of deformation. Zone I represents the behaviour of uncracked sample under increasing loading; it ends with the cracking of the matrix at the notch. Because of the specimen's less than critical fibre content, the reinforcement cannot bear the imposed high load after the matrix has cracked, so that a sudden drop in force (so-called "snap-back") occurs in Zone II. The magnitude of the "snap-back" depends mainly on the stiffness of test apparatus and bond characteristics between multi-filament yarn and matrix. Filaments with a very intensive bond to the matrix already fail in Zone II. The typical multi-filament yarn pullout takes place in Zone III, while as a rule deformation hardening can be observed. According to their bond characteristics, the single filaments are stretched in different manners during crack-opening [2,3]. With increasing load a successive failure of filaments occurs. After the strain-capacity is reached, the specimen behaviour is characterised by a pronounced softening.

For an easier comparison of the results obtained from the mechanical tests, pullout force vs. crack-opening curves were derived and presented instead of the complete load–deformation diagrams. This means that Zone I and Zone II of the curves are not shown in order to avoid overloading the graphs. Only in the cases when Zone II could not be distinguished from Zone III (continuous drop of curve, no strain hardening after a snap-back), the graph was depicted starting with Zone II. Each diagram gives characteristic pullout curves for a particular material composition (e.g., Fig. 5), while the duration of the accelerated aging in the fog chamber is always the variation parameter. Each of these characteristic curves was drawn using a "best-fit" method from up to 10 curves obtained from the individual tests. In order to quantify the pullout behaviour, three parameters were selected for the curve characterisation as shown in Fig. 4: maximum fibre pullout force F_{max}, fibre pullout work $W_{0.25}$ and $W_{0.5}$ at crack widths of 0.25 mm and 0.5 mm, respectively. The values of these parameters are given in a graph which always joins the corresponding diagram with the characteristic curves. In contrast to the characteristic curves, the parameters F_{max}, $W_{0.25}$ and $W_{0.5}$ are given for every measured curve in a corresponding diagram, so that also the scattering of the obtained values can be observed. Additionally the average values as well as the corresponding standard deviations are given in Table 3. In case of an indistinguishable Zone II and Zone III F_{max} could not be determined and pullout work was calculated beginning with Zone II.

Additionally to the diagrams, electron-microscopic images of the bonding area between multi-filament yarn and matrix are presented for selected duration of accelerated aging. The images illustrate typical morphology changes in this area due to aging.

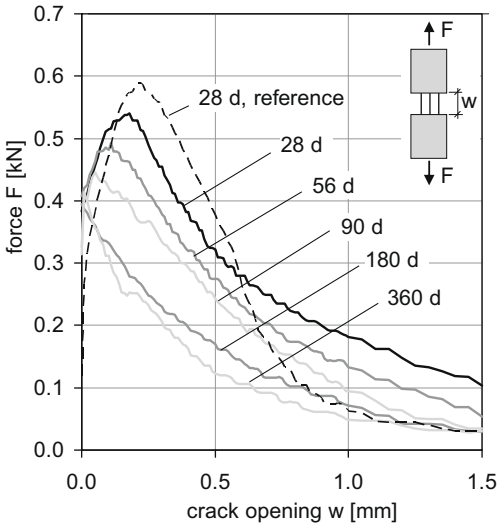

Fig. 5. Force vs. crack-opening curves for the specimens made of Matrix M1 and yarn VET-03; storage at 40 °C/99% RH, reference at 20 °C/65% RH.

4.2. Influence of matrix composition

The effects of matrix composition on the development of the mechanical performance of the specimens subjected to accelerated aging in a fog chamber were investigated in the first place.

Fig. 5 shows the characteristic pullout curves for the Matrix M1 samples (reduced alkalinity), which were reinforced with the multi-filament yarn VET-03. With increasing aging time in the fog chamber mechanical performance of the bond steadily decreases. Fig. 6 provides the values of the parameters derived from individual measurements and gives the corresponding non-linear regression curves. The maximum fibre pullout force F_{max} decreased by approximately 25% after one year of accelerated aging, while the work capacity $W_{0.25}$ and $W_{0.5}$ decreased by approximately 40% in comparison to the reference (specimens stored in the standard laboratory climate and tested at the age of 28 days). Fig. 11 illustrates the typical morphology of the interface zone between multi-filament yarn and Matrix M1. Along with matrix substances delicate products of hydration (CSH-phases) can be seen which have grown on the filament surfaces. At some spots, salient, very thin, shell-like hulls are to be found on the filaments.

Fig. 7 presents the characteristic pullout curves obtained for Matrix M7 specimens (high alkalinity), again reinforced with multi-filament yarn VET-03. In contrast to Fig. 5, significantly higher pullout forces F_{max} were measured for reference specimens (age 28 days, stored in the standard laboratory climate) in comparison to the corresponding tests with Matrix M1 (cf. Fig. 5). This can be traced back to a higher reactivity of the Matrix M7 binder (CEM I cement, no

Table 3
Average values and standard deviations (italics) of the maximum fibre pull-out force (F_{max}) and the pull-out work W up to crack widths of 0.25 mm ($W_{0.25}$) and 0.5 mm ($W_{0.5}$).

Matrix-yarn	Age																	
	Reference			28 d			56 d			90 d			180 d			360 d		
	F_{max} (N)	$W_{0.25}$ (N m)	$W_{0.5}$ (N m)	F_{max} (N)	$W_{0.25}$ (N m)	$W_{0.5}$ (N m)	F_{max} (N)	$W_{0.25}$ (N m)	$W_{0.5}$ (N m)	F_{max} (N)	$W_{0.25}$ (N m)	$W_{0.5}$ (N m)	F_{max} (N)	$W_{0.25}$ (N m)	$W_{0.5}$ (N m)	F_{max} (N)	$W_{0.25}$ (N m)	$W_{0.5}$ (N m)
M1-	620	0.28	0.48	540	0.25	0.43	490	0.23	0.39	455	0.19	0.32	420	0.16	0.27	435	0.16	0.25
VET-03	*68*	*0.06*	*0.04*	*42*	*0.01*	*0.01*	*37*	*0.01*	*0.03*	*59*	*0.03*	*0.06*	*57*	*0.02*	*0.06*	*43*	*0.03*	*0.07*
M3-	663	0.29	0.49	574	0.24	0.36	479	0.2	0.31	450	0.17	0.25	444	0.15	0.21	409	0.14	0.2
VET-03	*34*	*0.02*	*0.03*	*56*	*0.02*	*0.03*	*46*	*0.02*	*0.04*	*57*	*0.01*	*0.03*	*38*	*0.03*	*0.04*	*32*	*0.02*	*0.02*
M3-	691	0.3	0.47	536	0.19	0.28	456	0.15	0.19	442	0.12	0.16	387	0.09	0.12	–	0.05	0.07
VET-02	*223*	*0.03*	*0.03*	*60*	*0.02*	*0.04*	*53*	*0.02*	*0.05*	*67*	*0.02*	*0.03*	*50*	*0.02*	*0.02*	–	*0.01*	*0.02*
M7-	850	0.37	0.52	–	0.1	0.12	–	0.08	0.09	–	0.03	0.04	–	0.04	0.05	–	0.04	0.05
VET-03	*65*	*0.03*	*0.06*	–	*0.01*	*0.01*	–	*0.02*	*0.02*	–	*0.02*	*0.02*	–	*0.01*	*0.02*	–	*0.01*	*0.01*
M45-	603	0.25	0.51	547	0.25	0.45	531	0.23	0.44	530	0.24	0.46	507	0.24	0.41	0.84	0.23	0.4
VET-03	*51*	*0.03*	*0.03*	*37*	*0.02*	*0.04*	*84*	*0.04*	*0.08*	*45*	*0.03*	*0.06*	*47*	*0.02*	*0.04*	*43*	*0.02*	*0.05*

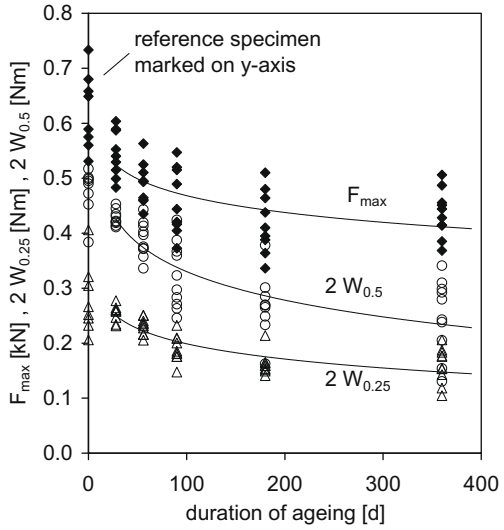

Fig. 6. Maximum pullout force F_{max} and pullout work $W_{0.25}$ and $W_{0.5}$ at the crack-opening of 0.25 mm and 0.5 mm, respectively, vs. duration of aging (Matrix M1, yarn VET-03).

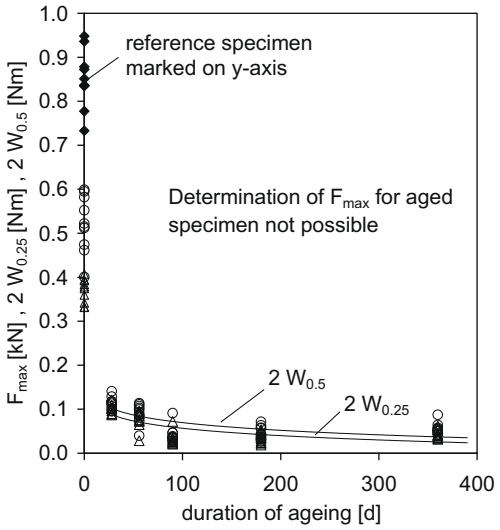

Fig. 8. Maximum pullout force F_{max} and pullout work $W_{0.25}$ and $W_{0.5}$ at the crack-opening of 0.25 mm and 0.5 mm, respectively, vs. duration of aging (Matrix M7, yarn VET-03).

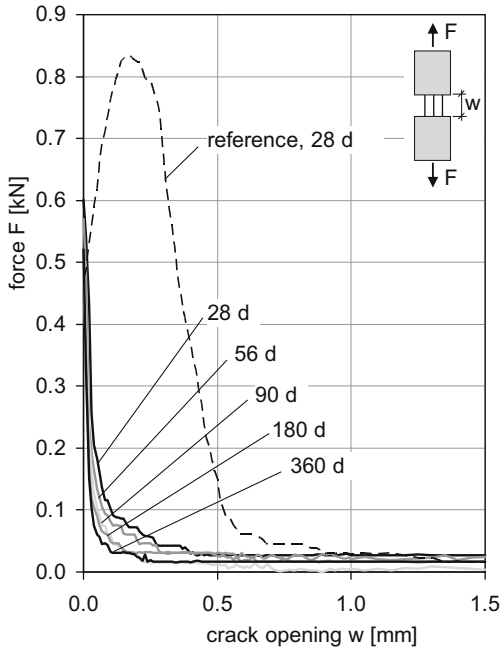

Fig. 7. Force vs. crack-opening curves for the specimens made of Matrix M7 and yarn VET-03; storage at 40 °C/99% RH, reference at 20 °C/65% RH.

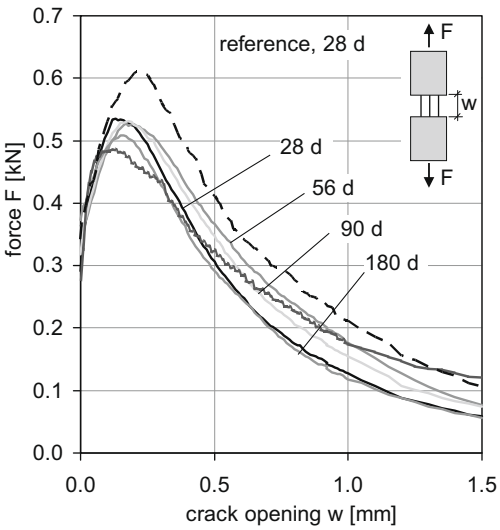

Fig. 9. Force vs. crack-opening curves for the specimens made of Matrix M45 and yarn VET-03; storage at 40 °C/99% RH, reference at 20 °C/65% RH.

addition of pozzolans). Furthermore, higher values of the work capacity $W_{0.25}$ and $W_{0.5}$ were obtained from the reference tests with Matrix M7. However, a dramatic worsening of the performance occurred due to 28 days aging already in the case when Matrix M7 was used. The force-crack opening curves indicate a brittle failure (cf. Fig. 7; very steep descending branch, F_{max} values could not be measured). Consequently, only very low pullout work could be noted (Fig. 8). The behaviour of the composite becomes even more brittle with increasingly long aging periods until nearly no crack-bridging by the reinforcement can be observed (cf. Figs. 7 and 8). The corresponding ESEM image of the fill-in zone (cf. Fig. 12) documents a massive precipitation of Portlandite ($Ca(OH)_2$) among the filaments already after 28 days' aging. Spindly hydration products, as observed with the use of Matrix M1 (cf. Fig. 11), can be only detected to a minimal extent. Thick, brittle shells of hydration products enveloping the filaments are dominant. The thickness of such shells increases with the duration of aging.

The pullout curves for Matrix M45 specimens (similar composition as Matrix M1 but with metakaoline instead of microsilica) reinforced with yarn VET-03 are presented in Fig. 9. The performance at the beginning of aging corresponds to that of Matrix M1. But in contrast very little change of the force-crack opening curves (Fig. 9) and nearly no losses in the maximum pullout force F_{max} as well as in the pullout work $W_{0.25}$ and $W_{0.5}$ (cf. Fig. 10) occurred after continued aging. Figs. 13 and 14 show the morphology at the fibre–matrix interface in the specimen subjected to an accelerated aging of 28 days' and 360 days' duration, respectively. Different hydration products partially envelop the filaments, mainly consisting of CSH phases and some ettringite-like needles (probably resulting from aluminates in metacaoline). No significant change of interface morphology due to aging is apparent.

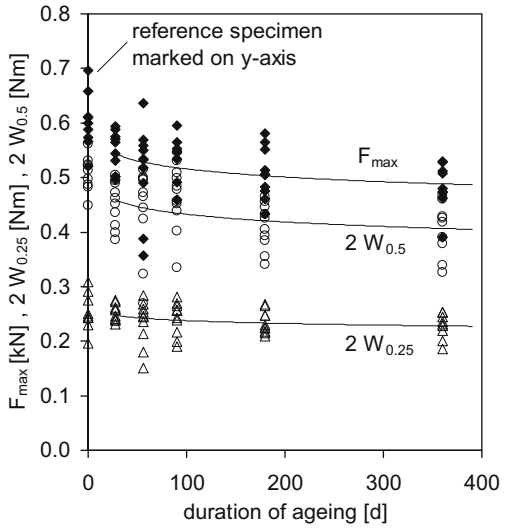

Fig. 10. Maximum pullout force F_{max} and pullout work $W_{0.25}$ and $W_{0.5}$ at the crack-opening of 0.25 mm and 0.5 mm, respectively, vs. duration of aging (Matrix M45, yarn VET-03).

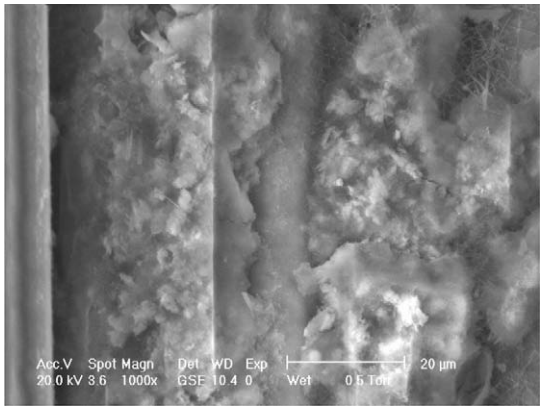

Fig. 11. ESEM image of VET-03 filaments in Matrix M1 after 360 days of accelerated aging.

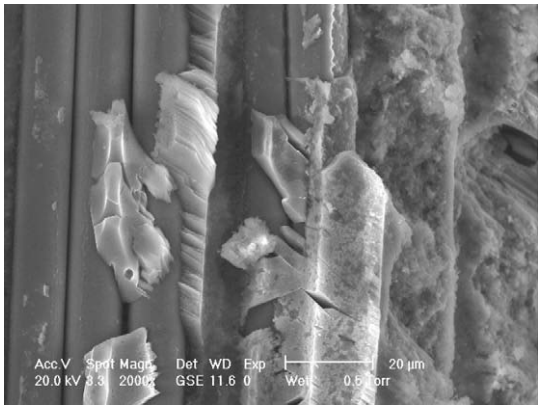

Fig. 12. ESEM image of VET-03 filaments in Matrix M7 after 28 days of accelerated aging.

The surfaces of filaments show no changes which are visible under the ESEM for any matrix composition. Thus a corrosive alteration of the surface, as found in [11,12], could not be established.

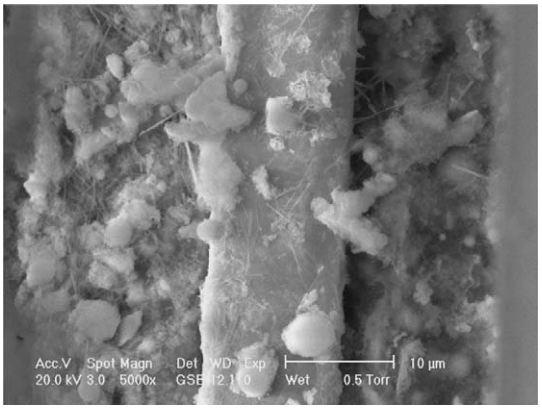

Fig. 13. ESEM image of VET-03 filaments in Matrix M45 after 28 days of accelerated aging.

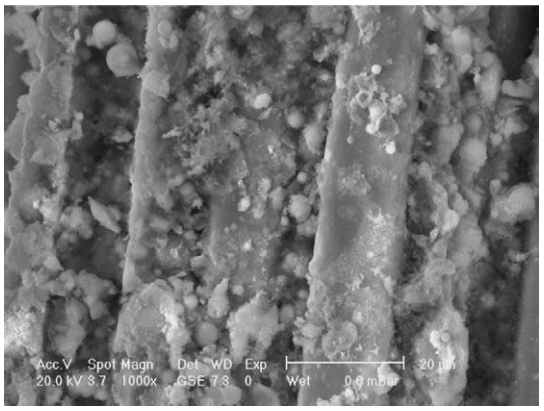

Fig. 14. ESEM image of VET-03 filaments in Matrix M45 after 360 days of accelerated aging.

Evaluation of the results allows the conclusion that the essential cause of the poor performance of the specimens made of Matrix M7 is the high pH level of the pore solution in this alkali-rich composition. This high level is perpetuated by the continuous new formation of Portlandite during aging since Portland cement continues hydrating in the moist environment of the fog chamber. No decomposition of $Ca(OH)_2$ by pozzolanic reactions take place in Matrix M7, and almost no carbonate formation from Portlandite occurs because of the high relative humidity (99%). The interfaces between matrix and filament and between individual filaments are thus determined by large, splittable Portlandite crystals and shells of hydration products, containing $Ca(OH)_2$ to a large extent. Already at small displacements of the filaments the Portlandite crystals as well as the brittle shells around the filaments tend to shatter, wedge themselves unfavourably, and exert notching at the filaments and lateral punctual pressure. Furthermore, chemo-mechanical notching at the fibre surface [11] as well as growth of surface defects (invisible in ESEM) may occur [29–33]. All these effects can lead, separately or in combination with one another, to failure of the filaments even at relatively low loads.

The differences in behaviour of specimens M1 and M45 cannot explained straightforwardly. The evolution of pH values over time shows only small differences and a crossover after 90 days of accelerated aging (cf. Fig. 1). Therefore, delayed failure due to the growth of surface defects can be excluded as the exclusive damaging process. The performance of Matrix M45 specimens would develop similar to that observed for Matrix M1 specimens, differing in nuances only (depending on disparities in OH^- concentration).

Also evident is that notching mechanisms as explained above for Matrix M7 cannot be explained. Rather different developments of interface structure seem to be responsible in turn for the different performance development between the specimens made of Matrices M1 and M45. Slight densifications of fibre/matrix interface can be observed in case of Matrix M1, while the micrographs for Matrix M45/filament interfaces showed no significant changes during aging. Some damaging of filaments due to the growth of surface defects can, of course, not be excluded, but it is surely not the only reason for performance losses of cementitious glass fibre composites.

4.3. Influence of the size composition

This section reports on the influence of the composition of polymeric sizing on filament surface on the development of the mechanical performance of the specimens subjected to accelerated aging in a fog chamber.

Figs. 15 and 17 show the force vs. crack-opening curves for specimens made of Matrix M3 (binder: Portland cement with an addition of pozzolans). Multi-filament yarns VET-03 (Fig. 15) and VET-02 (Fig. 17), respectively, were used as reinforcing fibre. Approximately 10% higher maximum fibre pullout force F_{max} could be observed for both yarn (i.e., size) qualities in comparison to the tests on the specimens made of Matrix M1 and yarn VET-03 (cf. Fig. 5) at the reference age of 28 days. However, the pullout work $W_{0.5}$ for the M3 based specimens is approximately 20% lower after 28 days of accelerated aging in comparison to corresponding values for the M1 based specimens (cf. Figs. 16 and 18 and Fig. 6). The higher fibre pullout forces for the M3 based specimens in the reference tests (age 28 days) can be attributed to the changes in the binder composition. The significantly higher Portland cement clinker proportion of Matrix M3 in comparison with Matrix M1 leads at first to a more rapid, more effective bonding of the filaments into the matrix. The increased content of Portlandite is at this age consumed by the pozzolans in the formation of CSH phases. However, the decomposition of Portlandite becomes slower with continuing aging in the fog chamber, since the content of pozzolanes decreases due to their consumption for the pozzolanic reactions. This explains the decrease in the performance of the aged M3 based specimens in comparison to the M1 based specimens.

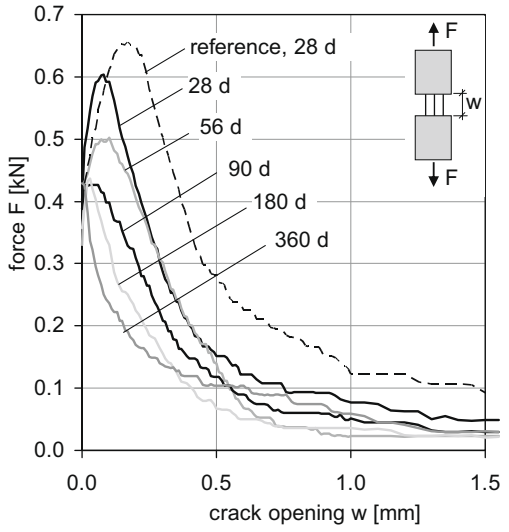

Fig. 15. Force vs. crack-opening curves for the specimens made of Matrix M3 and yarn VET-03; storage at 40 °C/99% RH, reference at 20 °C/65% RH.

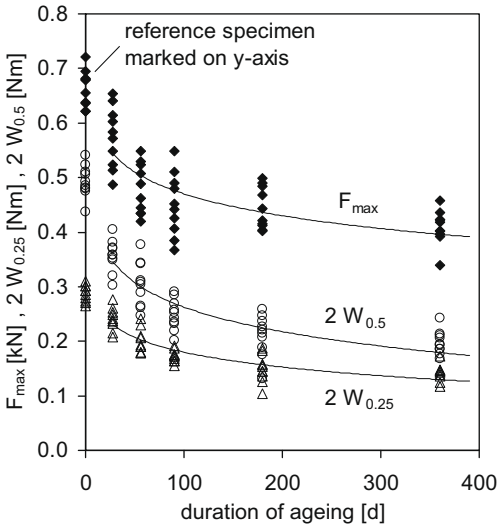

Fig. 16. Maximum pullout force F_{max} and pullout work $W_{0.25}$ and $W_{0.5}$ at the crack-opening of 0.25 mm and 0.5 mm, respectively, vs. duration of aging (Matrix M3, yarn VET-03).

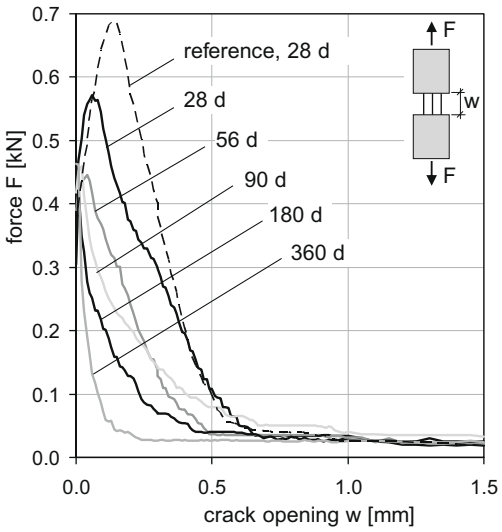

Fig. 17. Force vs. crack-opening curves for the specimens made of Matrix M3 and yarn VET-02; storage at 40 °C/99% RH, reference at 20 °C/65% RH.

Further development of mechanical performance with continuing aging differs considerably for the M3 specimens depending on the quality of the filament sizing, whose composition is unknown. The material combination of Matrix M3 and yarn VET-03 shows a 50% reduction in the pullout work $W_{0.5}$ (Fig. 16), while the samples made of Matrix M3 and yarn VET-02 exhibit after 360 days' storage in the fog chamber only 20% of the pullout work $W_{0.5}$ as measured for the reference storing conditions (Fig. 18).

Since all parameters in the investigation were identical, with the exception of the multi-filament yarns, and since the composition of bulk glass as well as the processing of filaments is supposed to be the same, the differences in the changes of the mechanical performance for the specimens made of Matrix M3 and multi-filament yarn VET-02 and VET-03, respectively, could be attributed solely to the different formulation of the fibre size, which, however, is not released by the fibre manufacturer. Laying degrees of responsibility for the performance losses in the composite material TRC as between the formation of new solid phases or to the degradation of

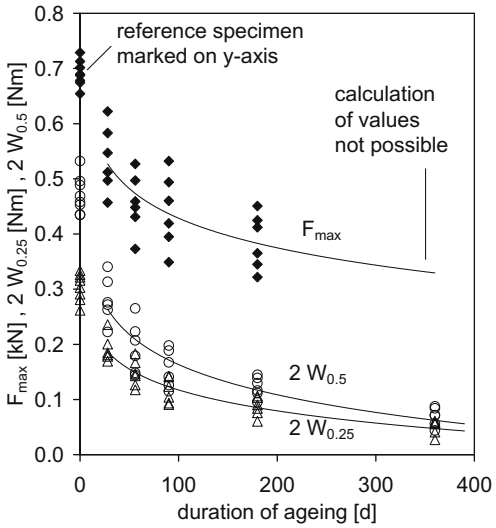

Fig. 18. Maximum pullout force F_{max} and pullout work $W_{0.25}$ and $W_{0.5}$ at the crack-opening of 0.25 mm and 0.5 mm, respectively, vs. duration of aging (Matrix M3, yarn VET-02).

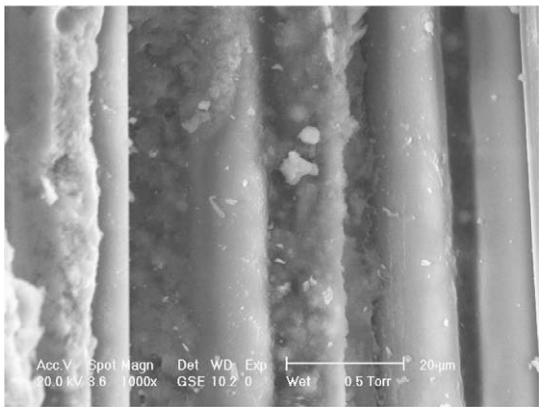

Fig. 19. ESEM image of VET-03 filaments in Matrix M3 after 28 days of accelerated aging.

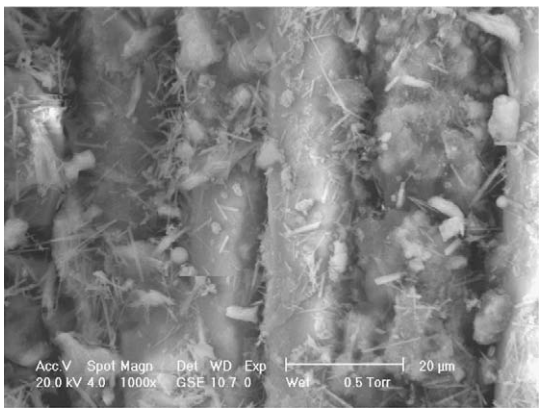

Fig. 20. ESEM image of VET-02 filaments in Matrix M3 after 28 days of accelerated aging.

the filaments' strength cannot be done cleanly. However, there is a clear effect of the size quality on the interface crystallisation. Fig. 19 (Matrix M3 and VET-03 fibre) and Fig. 20 (Matrix M3 and VET-02 fibre) illustrate this finding with images of filaments bonded to the matrix after 360 days of accelerated aging. Favourable microstructure for the bonding forms on the filament surfaces in the case of the fibre VET-03. The CSH phases dominate the morphology here. In the case of the fibre VET-02, in contrast, the filament shrouds are significantly less homogeneous, more coarsely structured, and interspersed with needle-like ettringite formations.

As stated before, it could not be determined if damaging effects were caused primary by the degradation of filaments (delayed failure) or rather by the development of the hydration phases in the fibre–matrix interface or, which seems most probable, by a combination of these two (and maybe also further) processes. However, the eminent influence of the polymeric filament sizing could be demonstrated here for the aging processes in TRC.

4.4. Discussion of the protective effect of the filament size

Evaluating the results at hand, it can be concluded that the established losses in the mechanical performance of the composites consisting of cement-based matrix and continuous glass fibre cannot result solely from delayed failure due to stress corrosion of fibre at defect tips. They are rather the result of both new formation of solid products on and among the filaments and losses in strength of filaments caused by defect growth. In the opinion of authors the first effect predominates in matrices adapted for the use in TRC.

It is also the authors' belief that the polymeric sizing of filaments heals existing defects originated from spinning and provides over a long time an additional protection of filament surface against nucleation of new surface defects caused by aggressive alkaline media. Fibre damage due to glass corrosion at individual sites on the filaments can of course not be excluded in this discussion. In the course of the extensive image investigations local damage to individual glass filaments in the imbedded multi-filament yarns (analogous to [12]) could be established in rare instances.

Visible surface defects as shown in Fig. 21 arises nearly always in a line parallel to the longitudinal axis of filament. This can be explained by the following hypothesis. The thickness of fibre size is non-uniform along the circumference of filament. During the winding of freshly sized filaments to strands, it was observed that a portion of the size is squeezed out somewhere between the strands if filaments are in direct contact to each other. A reduced thickness of size between the filaments is the result (cf. Fig. 22a). This state is conserved by thermal treatment of size. During further processing of multi-filament yarn, relative displacements of the filaments can take place. This can lead to separation of the lightly adhered filaments to a linear zone of size with reduced thickness (Fig. 22b). After embedding the multi-filament yarn in the cementitious matrix, the thickness of size is steadily reduced due to the aggressive environment, where the rate of loss in thickness de-

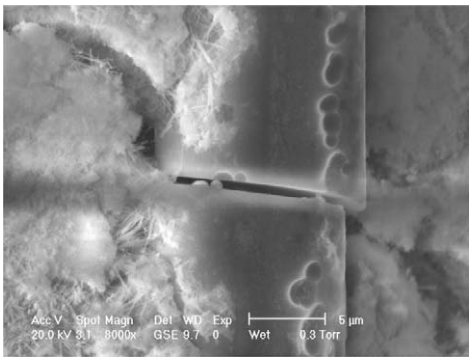

Fig. 21. Linear aligned corrosion spots on filaments VET-03 after 360 d exposure in water at 60 °C.

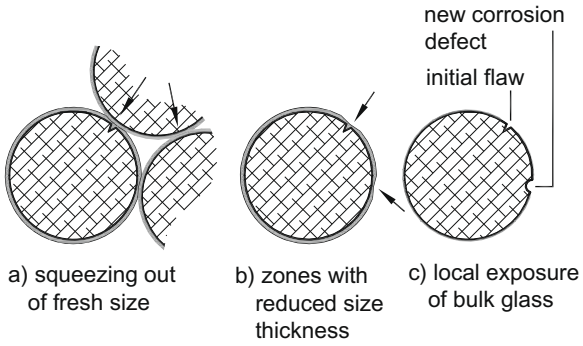

Fig. 22. Schematic view of processes leading to aligned corrosion spots on filament surface.

creases with duration of the exposure [25]. Logically, OH^- ions reach the glass fibre surface much more easily or earlier at the locations with reduced size thickness. If the glass has a disadvantageous composition locally (e.g., low ZrO_2 content) at certain line-like zones of glass exposure, corrosion of glass starts at these aligned spots. It must be emphasized that this kind of corrosion was detected in rare instances on filaments embedded in highly alkaline matrix and aged at elevated temperatures.

The mechanism described clearly points out the protective effect of filament size. Pronounced filament corrosion can take place only if the filament size is removed or strongly reduced in thickness. Stress corrosion on surface defects which originate from filament spinning thus becomes relatively improbable. These defects are filled with and covered by size [26]. The deterioration of size covering these flaws, due to its increased thickness, needs significantly more time than the complete deterioration of a thinner size layer at the undamaged surface. Thus, an effective diffusion obstruction of OH^- ions to the crack tip is provided by the size, such that delayed failure might be retarded significantly. The appearance of new flaws at undamaged filament surfaces appears more probable, provided that the size has deteriorated to a great extent locally or over larger areas. Then nanoscopic defects can arise and grow to a critical length.

Finally it should be considered that the influence of these separated defects of individual filaments on the load-bearing behaviour of the entire multi-filament yarns is estimated to be marginal since the neighbouring filaments can compensate the local failure taking over the local forces as assumed in [2,3].

5. Summary and conclusions

In this research project mechanisms leading to an alternation of the mechanical performance of textile-reinforced concrete (TRC) were investigated using two-sided pullout tests on slender notched specimens reinforced with a few multi-filament glass yarns. The mechanical performance of the bond was described in terms of the maximum pullout force F_{max} and the work capacity for crack-openings of 0.25 and 0.5 mm, respectively. The main parameters under investigation were the composition of the matrix binder and the quality of the filament size. The accelerated aging of the specimens was achieved by storing them in a fog chamber at elevated temperature.

It was found that the extent of the performance losses with increasing duration of aging depend primary on the alkalinity of the pore solution in the matrix. As a result of continuing hydration the filaments in the contact zone are increasingly covered by hydration products which morphology and chemical composition depend on the matrix binder. A stratum of thin CSH phases leading to good bonding characteristics dominates in the cases when the Portland cement clinker content of the binder is low and/or pozzolanic fines are used (low alkalinity of the pore solution). In contrast, coarse, brittle Portlandite phases prevail in the matrix compositions with only Portland cement as binder (high alkalinity of the pore solution).

With increasing potential for Portlandite formation in the matrices, i.e., with their increasing alkalinity, the thickness of the shells around filaments increases and so does the brittleness of these envelopes. Furthermore, amplified precipitation of $Ca(OH)_2$ between the filaments can be observed. Straining the filaments causes local spallings in and off the shells as well as the splitting of the $Ca(OH)_2$ crystals. It appears that the resulting singularities and lateral pressure caused by the wedged crystals act as notches and lead to a premature failure of the filaments.

In matrices rich in ground granulated blast furnace slag an accelerated reduction of the pH values of the pore solution occurs due to pozzolanic reactions. The formation of Portlandite is considerably limited, thus favourable interface microstructure forms. Such thinly walled coatings of the outer filaments allow a good, flawless bond to the matrix. However, in this case as well some densification of inner parts of multi-filament yarn occurs due to precipitated hydration products (CSH phases), leading mainly to reduced deformability of inner filaments and therefore to a reduction in the toughness of the embedded yarn. The use of metakaolin in combination with fly ash as pozzolans provided especially good results: due to long-term stable interface configuration nearly no changes in the mechanical performance of the specimens could be observed for the entire period of the accelerated aging.

The type of fibre size can pronouncedly influence the long-term performance of the composite. The size affects the crystallisation processes in the fibre–matrix interface and acts as a protective layer sheltering glass fibre from the corrosive pore solution. Flaws in the size and inconsistencies in the composition of the bulk glass as well as high pH values of the pore solution are necessary prerequisites for local damage to fibre made of AR-glass. Corrosion of glass filaments embedded in fine-grained concrete could be observed in this investigation only as rare exceptions.

Stress corrosion (delayed failure) at nanoscopic defects on filament surface becomes an important mechanism for damage if the size is widely removed at least at some areas of filament surface. The failure of individual filaments due to corrosion can likely be compensated by the redistribution of the load to neighbouring filaments. This means that the failure of a few filaments cannot significantly affect the load-bearing capacity of the multi-filament yarn.

The recent tensile tests by the authors on specimens made of textile-reinforced concrete and subjected to accelerated aging in fog confirmed the findings of this study, in which – for an easier interpretation of the results – just a few unidirectional yarns were used as reinforcement for each specimen. The results of the tests on TRC specimens will be published elsewhere.

Acknowledgements

The work was carried out under the aegis of the Collaborative Research Centre 528 “Textile Reinforcement for Structural Strengthening and Retrofitting” financed by the German Research Foundation.

References

[1] Brameshuber W, editor. Textile reinforced concrete. State-of-the-art report of RILEM Technical Committee 201-TRC; 2006.
[2] Ohno S, Hannant DJ. Modelling the stress–strain response of continuous fibre reinforced cement composites. ACI Mater J 1994;91(3):306–12.
[3] Jesse F, Will N, Curbach M, Hegger J. Flexural load-bearing behavior of textile-reinforced concrete. In: Dubey A, editor. Textile-reinforced concrete. Proc ACI fall convention. Kansas City, SP-250CD-5, 2008 (CD-Rom); 2005.

[4] Bartos PJM, Zhu W. Effect of microsilica and acrylic polymer treatment on the aging of GRC. Cement Concrete Compos 1996;18(1):31–9.
[5] Gao SL, Mäder E, Plonka R. Coatings for glass fibers in a cementitious matrix. Acta Mater 2004;52(16):4745–55.
[6] Weichold O, Möller M. A cement-in-poly (vinyl alcohol) dispersion for improved fibre–matrix adhesion in continuous glass–fibre reinforced concrete. Adv Eng Mater 2007;9(8):712–5.
[7] Gao SL, Mäder E, Plonka R. Nanocomposite coatings for healing surface defects of glass fibers and improving interfacial adhesion. Compos Sci Technol, in press. doi: 10.1016/j.compscitech.2007.10.009.
[8] Paul A. Chemical durability of glasses; a thermodynamic approach. J Mater Sci 1977;12(11):2246–68.
[9] Majumdar AJ, West JM, Larner LJ. Properties of glass fibres in cement environment. J Mater Sci 1977;12(5):927–36.
[10] Larner LJ, Speakman K, Majumdar AJ. Chemical interactions between glass fibres and cement. J Non-Cryst Solids 1976;20(1):43–74.
[11] Yilmaz V, Glasser F. Reaction of alkali-resistant glass fibres with cement. Part 2: durability in cement matrices conditioned with silica fume. Glass Technol 1991;32(4):138–47.
[12] Hempel S, Butler M. Microscopic investigations on durability of textile-reinforced concrete. In: Fernandes I, Guedes A, Noronha F, Teles M, dos Anjos Ribeiro M, editor. Proc 11th Euroseminar on microscopy applied to building materials, Porto (CD-ROM); 2007 .
[13] Otto WH. Relationship of tensile strength of glass fibers to diameter. J Am Ceram Soc 1955;38(3):122–5.
[14] Tomozawa M. Fracture of glasses. Annu Rev Mater Sci 1996;26:43–74.
[15] Metcalf AG, Schmitz GK. Mechanism of stress corrosion in *E*-glass fibres. Glass Technol 1972;13(1):5–16.
[16] Michalske TA, Freiman SW. A molecular mechanism for stress corrosion in vitreous silica. J Am Ceram Soc 1983;66(4):284–8.
[17] Stucke M, Majumdar AJ. Microstructure of glass fibre-reinforced cement composites. J Mater Sci 1976;11(6):1019–30.
[18] Bentur A, Diamond S. Aging and microstructure of glass fiber cement composite reinforced with different types of glass fibers. Durability Build Mater 1987;4(3):201–26.
[19] Laws V, Langley AA, West JM. The glass fibre/cement bond. J Mater Sci 1986;21(1):289–96.
[20] Katz A, Bentur A. Mechanisms and processes leading to changes in time in the properties of CFRC. Adv Cem Based Mater 1996;3(1):1–13.
[21] Bentur A. Role of interfaces in controlling durability of fiber-reinforced cements. J Mater Civil Eng 2000;12(1):2–7.
[22] Hempel R, Butler M, Hempel S, Schorn H. Durability of textile-reinforced concrete. In: Proc international RILEM workshop on high performance fiber reinforced cementitious composites in structural applications, New York (CD-ROM); 2005.
[23] Zhu W, Bartos PJM. Assessment of interfacial microstructure and bond properties in aged GRC using a novel microindentation method. Cem Concr Res 1997;27(11):1701–11.
[24] Scherer GW. Crystallization in pores. Cem Concr Res 1999;29(8):1347–58.
[25] Mäder E, Plonka R, Schiekel M, Hempel R. Coatings on alkali-resistant glass fibres for the improvement of concrete. J Ind Text 2004;33(3):191–207.
[26] Zinck P, Pay MF, Rezakhanlou R, Gerard JF. Mechanical characterisation of glass fibres as an indirect analysis of the effect of surface treatment. J Mater Sci 1999;34(9):2121–33.
[27] Zinck P, Mäder E, Gerard JF. Role of silane coupling agent and polymeric film former for tailoring glass fiber sizings from tensile strength measurements. J Mater Sci 2001;36(21):5245–52.
[28] Litherland KL, Oakley DR, Proctor BA. The use of accelerated aging procedures to predict the long term strength of GRC composites. Cem Concr Res 1981;11(2):455–66.
[29] Purnell P, Short NR, Page CL. A static fatigue model for the durability of glass fibre reinforced cement. J Mater Sci 2001;36(22):5385–90.
[30] Purnell P, Beddows J. Durability and simulated aging of new matrix glass fibre reinforced concrete. Cem Concr Compos 2005;27(9–10):875–84.
[31] Orlowsky J, Raupach M, Cuypers H, Wastiels J. Durability modelling of glass fibre reinforcement in cementitious environment. Mater Struct 2005;38(2):155–62.
[32] Orlowsky J, Raupach M. Modelling the loss in strength of AR-glass fibres in textile-reinforced concrete. Mater Struct 2006;39(6):635–43.
[33] Orlowsky J, Raupach M. Durability model for AR-glass fibres in textile-reinforced concrete. Mater Struct 2008;41(7):1225–33.
[34] Purnell P, Short NR, Page CL, Majumdar AJ. Microstructural observations in new matrix glass fibre reinforced cement. Cem Concr Res 2000;30(11):1747–53.
[35] Butler M. Zur Dauerhaftigkeit von Verbundwerkstoffen aus zementgebundenen Matrices und alkaliresistenten Glasfaser-Multifilamentgarnen. Dissertation at the Institute of Construction Materials, TU Dresden; 2009 [in German].
[36] Glinicki MA, Brandt AM. Quantification of glass fibre–cement interfacial properties by SEM-based push-out test. In: Reinhardt HW, Naaman AE, editor. Proc 5th int RILEM workshop high performance fiber reinforced cement composites, Mainz, Proc 53 RILEM; 2007. p. 343–55.